Open access • Journal Article • DOI:10.1080/02726340600570377

A Full-Wave Homogenization Technique for Steel Fiber Reinforced Concrete

Stephan Van Damme, Ann Franchois

Institutions: Ghent University

Published on: 19 Aug 2006 - Electromagnetics (Taylor & Francis Group)

Topics: Fiber-reinforced concrete, Reinforced solid and Homogenization (chemistry)

Electromagnetics, 26:301–314, 2006

ISSN: 0272-6343 print/1532-527X online
DOI: 10.1080/02726340600570377

Taylor & Francis
Taylor & Francis Group

A Full-Wave Homogenization Technique for Steel Fiber Reinforced Concrete

STEPHAN VAN DAMME
ANN FRANCHOIS

Electromagnetics Group
Department of Information Technology (INTEC-IMEC)
Ghent University
Ghent, Belgium

In steel fiber reinforced concrete, steel fibers are randomly oriented in the concrete host. This article presents a full-wave homogenization technique for the computation of the effective permittivity of perfectly conducting wires embedded in a dielectric host. The technique is illustrated with numerical examples and is compared with predictions from a classical mixing formula.

Keywords random media, effective permittivity, electromagnetic homogenization, method of moments, concrete

Introduction

Steel fiber reinforced concrete (SFRC) is obtained by mixing steel fibers with the fresh concrete, e.g., in a truck mixer. This type of reinforcement has excellent isotropic mechanical properties and is mainly used for slabs on grade such as industrial floors. Depending on the application, the length l and diameter d of the fiber typically are chosen in the ranges 10 mm $< l <$ 80 mm and 0.1 mm $< d <$ 1 mm. The fiber content determines the strength and ranges from 20 kg/m^3 to 80 kg/m^3, which corresponds to a volume fraction f_v between 0.002 and 0.01. At present an inspection of the fiber content accross the slab is done in a destructive way by drilling out cores, crushing them, and counting the number of fibers (Taerwe et al., 1999). Recently a nondestructive microwave measurement technique to determine the fiber content was developed (Van Damme et al., 2004). This technique combines an open-ended coaxial probe reflectometry method, in order to measure the effective permittivity of the SFRC, with a Maxwell–Garnett type of mixing formula, in order to derive the fiber content from the measured effective permittivity. Although classical mixing formulas have their merits, their applicability in terms of volume fractions, inclusion geometry, and frequency is limited.

In this paper a full-wave homogenization technique is presented. It is then possible to study the relationship between the effective permittivity and the fiber content in an

Received 6 January 2005; accepted 24 March 2005.
The authors are grateful to Prof. Luc Taerwe for his advice on SFRC. This work was sponsored by the Fund for Scientific Research—Flanders (Belgium).
Address correspondence to Ann Franchois, Electromagnetics Group, Department of Information Technology, Ghent University, Ghent, Belgium. E-mail: ann.franchois@ugent.be

exact way. The SFRC is considered as a uniform distribution of identical perfectly electrically conducting (PEC) wires, which are randomly oriented in a dielectric host. The effective permittivity of this wire medium is obtained by first computing the scattered field for a volume of wire medium surrounded with the homogeneous dielectric host and next by fitting to these data the permittivitty of a homogeneous volume with the same shape and dimensions and surrounded with the same dielectric host. In this paper cylindrically and spherically shaped volumes are considered. Similar approaches have been proposed by Sarabandi and Siqueira (1997) and Siqueira and Sarabandi (2000) for the homogenization of dense random media of dielectric spherical particles. The characterization of a two-dimensional plane composed of randomly distributed conducting sticks is reported in Nguyen and Mazé-Merceur (1998).

In the following sections, the homogenization approach and the full-wave solution technique are described, the analytical solutions and the Maxwell–Garnett mixing rule are given, and numerical results are discussed.

Homogenization Approach

A uniform distribution of randomly oriented identical straight PEC wires with length l and diameter d is considered. The wires are embedded in a homogeneous host medium with relative permittivity $\varepsilon_{r,h}$. The relative effective permittivity $\varepsilon_{r,eff}$ of the wire medium is defined by

$$\langle \mathbf{D} \rangle = \varepsilon_0 \varepsilon_{r,eff} \langle \mathbf{E} \rangle, \tag{1}$$

where ε_0 is the permittivity of vacuum and where $\langle\ \rangle$ denotes a spatial averaging of the macroscopic electric field $\mathbf{E}$ and electric induction $\mathbf{D}$ over a volume that contains a sufficiently large number of wires. Let V_s be the smallest such volume. In order to determine $\varepsilon_{r,eff}$, a finite volume of wire medium $V > V_s$ is surrounded with the homogeneous relative permittivity $\varepsilon_{r,h}$. In this paper V is a cylinder with radius a and height $H \gg a$ (Figure 1a) or a sphere with radius a (Figure 1b), where a is sufficiently large with respect to l. The position and orientation of wire i, $i = 1, \ldots, N$, are determined by its midpoint $\mathbf{m}_i$, elevation angle θ_i, and azimuth angle φ_i, where N is the total number of wires in V (Figure 2). The uniform distribution of the positions $\mathbf{m}_i$ is numerically realized by distributing a number of points, which corresponds to a given volume fraction f_v of the wires, uniformly within a cube that contains V and by keeping those points that lie within or on the surface of V. The random orientation of the wires is obtained with a sphere point picking method (Weisstein, 1999), which generates a uniform distribution of points on a spherical surface. It is well known that the elementary area element of a unit sphere in spherical coordinates, $d\Omega = \sin\theta d\theta d\varphi$, depends on θ. In order for any $d\Omega$ to contain the same density of points, the orientation angles φ_i and θ_i are chosen according to

$$\varphi = 2\pi u, \tag{2}$$

$$\theta = \cos^{-1}(2v - 1), \tag{3}$$

where u and v are uniformly distributed on the interval [0,1].

Next consider the same volume V, but filled with a homogeneous medium with relative permittivity $\varepsilon_{r,x}$ and also surrounded with the relative permittivity $\varepsilon_{r,h}$. In the

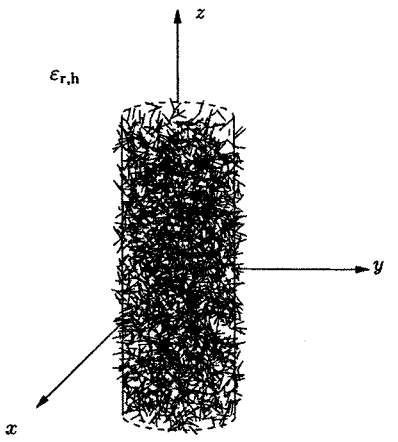

(a)

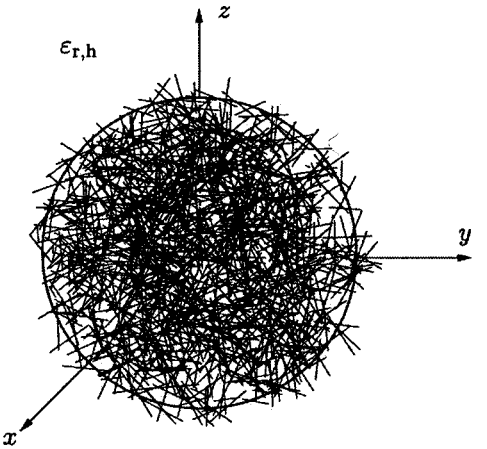

(b)

Figure 1. Wire medium cylinder (a) and sphere (b).

following, these volumes will be referred to as V_{wire} and V_{hom}, respectively. Both V_{wire} and V_{hom} are illuminated with the same given time-harmonic incident field $\mathbf{E}^i(\mathbf{r})$—the time dependence $\exp(j\omega t)$ will be omitted—and the respective scattered fields $\mathbf{E}^s_{wire}(\mathbf{r})$ and $\mathbf{E}^s_{hom}(\mathbf{r}, \varepsilon_{r,x})$ are computed in a number of observation points $\mathbf{r}_q$, $q = 1, \ldots, Q$, exterior to V. The relative permittivity $\varepsilon_{r,x}$ of V_{hom} which minimizes the root-mean-square error between $\mathbf{E}^s_{hom}(\mathbf{r}, \varepsilon_{r,x})$ and $\mathbf{E}^s_{wire}(\mathbf{r})$ over the set of observation points can be considered as the relative effective permittivity $\varepsilon_{r,eff}$ of the wire medium. Due to the statistical nature of V_{wire}, some kind of averaging has to be performed in order to obtain the coherent part of $\mathbf{E}^s_{wire}(\mathbf{r})$. This is typically done by taking the average scattered field for different random realizations of V_{wire} (Siqueira & Sarabandi, 2000). In this paper the rotational symmetry of V is exploited, hence just one random realization of V_{wire} is rotated to P different angles around the symmetry axis, with the incident field remaining unchanged.

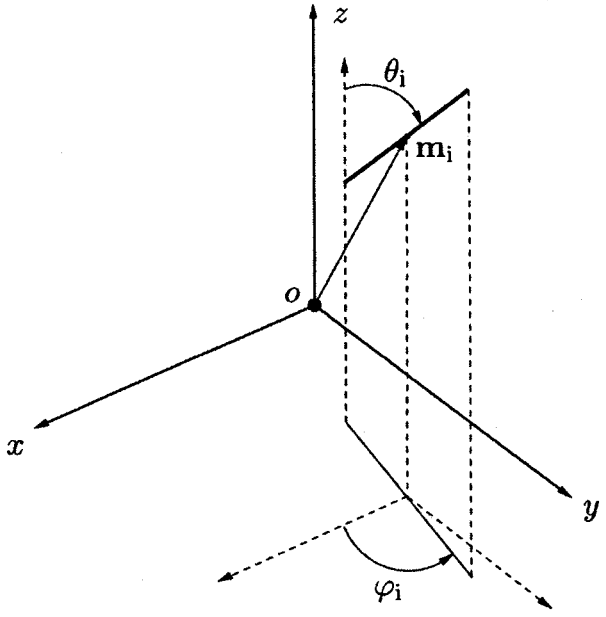

Figure 2. Wire coordinates.

The average scattered field is then given by

$$\langle \mathbf{E}^s_{wire,p}(\mathbf{r}_q)\rangle_p = \frac{1}{P}\sum_{p=1}^{P} \mathbf{E}^s_{wire,p}(\mathbf{r}_q). \tag{4}$$

The relative effective permittivity thus is obtained by minimizing a cost function

$$\mathcal{F}(\varepsilon_{r,x}) = \sum_{q=1}^{Q} |\langle \mathbf{E}^s_{wire,p}(\mathbf{r}_q)\rangle_p - \mathbf{E}^s_{hom}(\mathbf{r}_q, \varepsilon_{r,x})|^2. \tag{5}$$

In this paper, the incident field is a plane wave and the observation points $\mathbf{r}_q$ are regularly spaced on a circle with radius $b > a$ surrounding V, either in the near or in the far field of V. Details on the numerical computation of the scattered fields $\mathbf{E}^s_{wire}$ and $\mathbf{E}^s_{hom}$ are given in the following sections. The cost function (5) is minimized with a Levenberg–Marquardt algorithm (Press et al., 1988).

Note that the average scattered field (4) is obtained equivalently by keeping V_{wire} fixed and by rotating the incident field around the symmetry axis. Such a description, with P incident plane waves, will be adopted in the following:

$$\mathbf{E}^i_p(\mathbf{r}) = \mathbf{E}_0 \exp(-jk_h \mathbf{u}_p \cdot \mathbf{r}), \tag{6}$$

where $\mathbf{E}_0$ is a linearly polarized complex vector, $\mathbf{u}_p$ is the direction of propagation, and $k_h = k_0\sqrt{\varepsilon_{r,h}}$ and k_0 are the wavenumbers of the host medium and vacuum, respectively.

The following conventions are adopted for the respective configurations of the cylinder and sphere. The axis of the cylinder is along z. The incident field propagation directions are parallel to the xy-plane and are defined by $\mathbf{u}_p = (-\cos\varphi_p, -\sin\varphi_p, 0)$,

with $\varphi_p = (p-1)2\pi/P$, $p = 1, \ldots, P$. The polarization is parallel to z, hence $\mathbf{E}_0 = E_0\mathbf{u}_z$. The observation points are on a circle in the xy-plane; their coordinates are $\mathbf{r}_q = (b\cos\varphi_q, b\sin\varphi_q, 0)$, with $\varphi_q = (q-1)2\pi/Q$, $q = 1, \ldots, Q$. For the sphere, the incident field propagation directions are parallel to the yz-plane and are defined by $\mathbf{u}_p = (0, \sin\theta_p, \cos\theta_p)$, with $\theta_p = (p-1)2\pi/P$ and with $\varphi_p = \frac{\pi}{2}$, $p = 1, \ldots, P$. The polarization is parallel to x, hence $\mathbf{E}_0 = E_0\mathbf{u}_x$. The observation points are on a circle lying in a plane defined by the vectors $\mathbf{u}_x$ and $\mathbf{u}_p$. Their coordinates are given by $\mathbf{r}_q = (b\sin\xi_q, b\sin\theta_p\cos\xi_q, b\cos\theta_p\cos\xi_q)$, with $\xi_q = (q-1)2\pi/Q$, $q = 1, \ldots, Q$.

Full-Wave Solution for the Wire Medium Volume

For the computation of the field $\mathbf{E}^s_{wire}(\mathbf{r})$ scattered by the PEC wire medium volume V_{wire} an electric field integral equation formulation is applied. Since the aspect ratio l/d of the wires is large, a thin wire approximation can be used. This assumes that (i) the current on the surface of the wire is in the axial direction and does not show a circumferential variation, (ii) this current can be represented by a filamentary current $I(s)$ on the wire axis, with s a distance parameter along this axis, and (iii) the boundary condition of the electric field needs to be enforced in the axial direction only. The following equation in the unknown filamentary current $I(s)$ is obtained for one wire (Burke and Poggio, 1981):

$$-\mathbf{E}^i(\mathbf{r})\cdot\mathbf{u}_s = -\frac{jZ_h}{k_h}\int_0^l I(s')\left[k_h^2 - \frac{\partial^2}{\partial s'\partial s}\right]\left(\frac{e^{-jk_h|\mathbf{r}-\mathbf{r}'|}}{4\pi|\mathbf{r}-\mathbf{r}'|}\right)ds', \tag{7}$$

where $\mathbf{r}$ is an observation point on the surface of the wire, $\mathbf{r}'$ is a source point on the wire axis, $\mathbf{u}_s$ is the unit vector tangent to the wire axis, and $Z_h = Z_0/\sqrt{\varepsilon_{r,h}}$ is the impedance of the host medium, with $Z_0 = \sqrt{\mu_0/\varepsilon_0}$. The corresponding equation for the N wires in V_{wire} is given by

$$-\mathbf{E}^i(\mathbf{r}_i)\cdot\mathbf{u}_{s,i} = -\frac{jZ_h}{k_h}\sum_{j=1}^{N}\int_0^l I_j(s')\left[k_h^2\mathbf{u}_{s,i}\cdot\mathbf{u}_{s,j} - \frac{\partial^2}{\partial s'\partial s}\right]\left(\frac{e^{-jk_h|\mathbf{r}_i-\mathbf{r}'_j|}}{4\pi|\mathbf{r}_i-\mathbf{r}'_j|}\right)ds', \tag{8}$$

where $\mathbf{r}_i$ is an observation point on the surface of wire i and $\mathbf{r}'_j$ is a source point on the axis of wire j. Equation (8) is discretized with a Galerkin method of moments (Harrington, 1968) with sinusoidal basis and testing functions. The unknown current $I_j(s')$ on wire j is expanded as

$$I_j(s') = \sqrt{\frac{2}{l}}\sum_{n=1}^{N_b} I_{j,n}\sin\left(\frac{n\pi s'}{l}\right), \tag{9}$$

where N_b is the number of basis functions and $I_{j,n}$ are the unknown current coefficients. Testing (8) along all wires $\mathbf{r}_i$, $i = 1, \ldots, N$, with functions $\sqrt{2/l}\sin(m\pi s/l)$, $m = 1, \ldots, N_b$, then leads to a matrix equation

$$\overline{\overline{\mathbf{Z}}}\mathbf{I} = \mathbf{V}, \tag{10}$$

where $\mathbf{I} = [I_{1,1}\cdots I_{1,N_b}\cdots I_{N,1}\cdots I_{N,N_b}]^T$ is the vector of unknowns and $\mathbf{V} = [V_{1,1}\cdots V_{1,N_b}\cdots V_{N,1}\cdots V_{N,N_b}]^T$ is the excitation vector, which depends on the choice of the

incident field. Since there are P incident fields, as specified in the previous section, (10) is to be solved for P right-hand sides $\mathbf{V}^p$, where

$$V_{i,m}^p = K_{i,p} \int_0^l e^{j\alpha_{i,p}s} \sin\left(\frac{m\pi s}{l}\right) ds, \tag{11}$$

with

$$K_{i,p} = \sqrt{\frac{2}{l}} E_0 \cos\theta_i e^{jk_h[\cos\varphi_p(m_{i,x}-\frac{l}{2}\sin\theta_i\cos\varphi_i)+\sin\varphi_p(m_{i,y}-\frac{l}{2}\sin\theta_i\sin\varphi_i)]}, \tag{12}$$

$$\alpha_{i,p} = k_h[\cos\varphi_p \sin\theta_i \cos\varphi_i + \sin\varphi_p \sin\theta_i \sin\varphi_i] \tag{13}$$

for the cylinder and

$$K_{i,p} = \sqrt{\frac{2}{l}} E_0 \sin\theta_i \cos\varphi_i e^{-jk_h[\sin\theta_p(m_{i,y}-\frac{l}{2}\sin\theta_i\sin\varphi_i)+\cos\theta_p(m_{i,z}-\frac{l}{2}\cos\theta_i)]}, \tag{14}$$

$$\alpha_{i,p} = -k_h[\cos\theta_p \cos\theta_i + \sin\theta_p \sin\theta_i \sin\varphi_i] \tag{15}$$

for the sphere. With $\beta_m = m\pi/l$, (11) finally is expressed as

$$V_{i,m}^p = -\frac{K_{i,p}}{2}\left[\frac{e^{j(\alpha_{i,p}+\beta_m)l}}{\alpha_{i,p}+\beta_m} - \frac{e^{j(\alpha_{i,p}-\beta_m)l}}{\alpha_{i,p}-\beta_m} - \frac{1}{\alpha_{i,p}+\beta_m} + \frac{1}{\alpha_{i,p}-\beta_m}\right]. \tag{16}$$

The elements of the interaction matrix $\overline{\overline{\mathbf{Z}}}$ are given by

$$\begin{aligned} Z_{i,m,j,n} = {} & \frac{jZ_h}{k_h}\frac{2}{l}\int_0^l\int_0^l \sin\left(\frac{n\pi s'}{l}\right)\sin\left(\frac{m\pi s}{l}\right) \\ & \times\left[k_h^2 \mathbf{u}_{s,i}\cdot\mathbf{u}_{s,j} - \frac{\partial^2}{\partial s'\partial s}\right]\left(\frac{e^{-jk_h|\mathbf{r}_i-\mathbf{r}'_j|}}{4\pi|\mathbf{r}_i-\mathbf{r}'_j|}\right) ds'\,ds. \end{aligned} \tag{17}$$

For the mutual interactions, i.e., interactions between different wires $i \neq j$, the integrations in (17) are performed with 9- and 10-point Gaussian quadrature formulas. The elements of $\overline{\overline{\mathbf{Z}}}$ corresponding to the self interactions, hence $i = j$, can be written as

$$\begin{aligned} Z_{i,m,i,n} = {} & jZ_h k_h \frac{2}{l}\int_0^l\int_0^l \sin\left(\frac{n\pi s'}{l}\right)\sin\left(\frac{m\pi s}{l}\right)\frac{e^{-jk_h\sqrt{(s-s')^2+\left(\frac{d}{2}\right)^2}}}{4\pi\sqrt{(s-s')^2+\left(\frac{d}{2}\right)^2}} ds'\,ds \\ & - \frac{jZ_h}{k_h}\frac{2}{l}\left(\frac{n\pi}{l}\right)\left(\frac{m\pi}{l}\right)\int_0^l\int_0^l \cos\left(\frac{n\pi s'}{l}\right)\cos\left(\frac{m\pi s}{l}\right) \\ & \times\frac{e^{-jk_h\sqrt{(s-s')^2+\left(\frac{d}{2}\right)^2}}}{4\pi\sqrt{(s-s')^2+\left(\frac{d}{2}\right)^2}} ds'\,ds. \end{aligned} \tag{18}$$

The numerical integration of (18) is difficult due to the quasi-singular behavior around $s = s'$. Therefore, a transformation of variables is applied (Milovanovi & Velikovi, 2001):

$$s = \tau_2, \tag{19}$$

$$s - s' = \frac{d}{2}\sinh\tau_1, \tag{20}$$

leading to the following expressions for the integrals in (18):

$$\frac{1}{4\pi}\int_0^l \int_{\sinh^{-1}\left(\frac{\tau_2-s}{d/2}\right)}^{\sinh^{-1}\left(\frac{\tau_2}{d/2}\right)} \left\{\begin{matrix}\sin\\ \cos\end{matrix}\right\}\left(\frac{n\pi(\tau_2 - \frac{d}{2}\sinh\tau_1)}{l}\right) \left\{\begin{matrix}\sin\\ \cos\end{matrix}\right\}\left(\frac{m\pi\tau_2}{l}\right) e^{-jk_h\frac{d}{2}\cosh\tau_1}\, d\tau_1\, d\tau_2. \tag{21}$$

The integrands are now well behaved and are computed as with the mutual interactions.

The computation of the interaction matrix elements (17) is time consuming, especially when the number of wires is large. Therefore, an approximation is introduced for the interactions between wires $i \neq j$ that are sufficiently distant from each other. It consists of replacing the distance $|\mathbf{r}_i - \mathbf{r}'_j|$ in (17) with the constant distance $R_{i,j} = |\mathbf{m}_i - \mathbf{m}_j|$ between the midpoints of both wires, yielding

$$\begin{aligned} Z_{i,m,j,n} &= jZ_h k_h \frac{2}{l}\left(\frac{2l}{\pi}\right)^2 \frac{1}{nm}\frac{e^{-jk_h R_{i,j}}}{4\pi R_{i,j}}\mathbf{u}_{s,i}\cdot\mathbf{u}_{s,j} \qquad \text{for } m \text{ and } n \text{ odd} \\ &= 0 \qquad \text{otherwise.} \end{aligned} \tag{22}$$

Numerical experiments showed that this approximation can be used for $R_{i,j} > 7l$ at frequencies below 1 GHz. The relative error between the exact and the approximate integration is then smaller than 1%. In this paper, (10) is solved with a direct backsubstitution method with multiple right-hand sides from MATLAB.

Once the current coefficients $\mathbf{I}^p$ are solved, the scattered field is computed with

$$\begin{aligned} \mathbf{E}_p^s(\mathbf{r}) = &-j\omega\mu_0\sqrt{\frac{2}{l}}\sum_{j=1}^{N}\sum_{n=1}^{N_b} I_{j,n}^p \int_0^l \sin\left(\frac{n\pi s'}{l}\right)\frac{e^{-jk_h|\mathbf{r}-\mathbf{r}'_j|}}{4\pi|\mathbf{r}-\mathbf{r}'_j|}\, ds'\, \mathbf{u}_{s,j} \\ &+ \frac{1}{j\omega\varepsilon_h}\sqrt{\frac{2}{l}}\sum_{j=1}^{N}\sum_{n=1}^{N_b} I_{j,n}^p \int_0^l \frac{n\pi}{l}\cos\left(\frac{n\pi s'}{l}\right)\nabla\left(\frac{e^{-jk_h|\mathbf{r}-\mathbf{r}'_j|}}{4\pi|\mathbf{r}-\mathbf{r}'_j|}\right) ds'. \end{aligned} \tag{23}$$

Analytical Solutions for the Homogeneous Cylinder and Sphere

The field $\mathbf{E}^s_{hom}(\mathbf{r})$ scattered by the homogeneous cylinder V_{hom} with radius a and height H is approximated by the analytical solution for the two-dimensional infinitely long cylinder. For a cylinder with relative permittivity $\varepsilon_{r,x}$ in a host medium $\varepsilon_{r,h}$ (Figure 3a) that is illuminated with a linearly polarized plane wave $\mathbf{E}^i = E_0 e^{jk_h x}\mathbf{u}_z$, the scattered

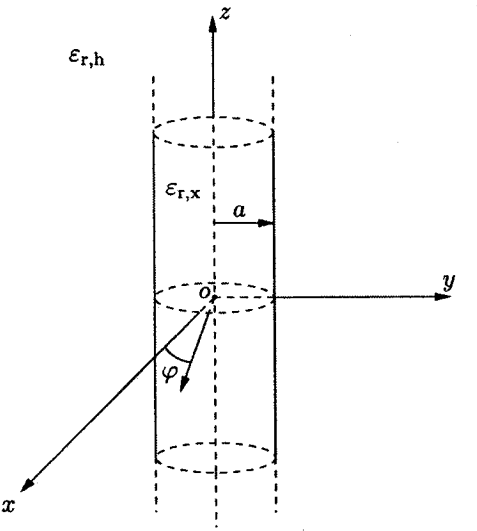

(a)

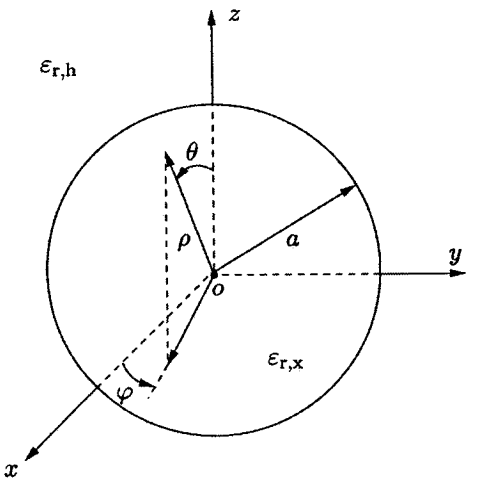

(b)

Figure 3. Homogeneous cylinder (a) and sphere (b).

field on a circle with radius $b > a$ is given by (Harrington, 2001)

$$E^s_{hom}(b, \varphi_q) = E_0 \sum_{n=-\infty}^{\infty} j^n a_n H_n^{(2)}(k_h b) e^{jn\varphi_q}, \tag{24}$$

with

$$a_n = \frac{k_h J_n(k_x a) J_n'(k_h a) - k_x J_n(k_h a) J_n'(k_x a)}{k_h J_n(k_x a) H_n'^{(2)}(k_h a) - k_x H_n^{(2)}(k_h a) J_n'(k_x a)}, \tag{25}$$

where $k_x = k_0\sqrt{\varepsilon_{r,x}}$ and $J_n(x)$ and $H_n^{(2)}(x)$ are the Bessel function of the first kind and the Hankel function of the second kind, of order n, respectively. As is shown further, this two-dimensional approximation yields satisfactory results provided that $H \gg a$ and that b is not much larger than a.

For a homogeneous dielectric sphere V_{hom} with radius a and relative permittivity $\varepsilon_{r,x}$ in a host medium $\varepsilon_{r,h}$ (Figure 3b), that is illuminated with a linearly polarized plane wave $\mathbf{E}^i = E_0 e^{-jk_h z}\mathbf{u}_x$, the scattered field in a point (ρ, θ, φ) with $\rho > a$ is given by (Van Bladel, 1985)

$$\mathbf{E}^s(\rho,\theta,\varphi) = \nabla \times \nabla(v^s \rho \mathbf{u}_\rho) - j\omega\mu\nabla \times (w^s \rho \mathbf{u}_\rho), \tag{26}$$

$$v^s = \frac{j}{k}\sum_{n=1}^{\infty}(-j)^n \frac{2n+1}{n(n+1)}\cos\varphi P_n^1(\cos\theta)[j_n(k_h\rho) - a_n h_n^{(2)}(k_h\rho)], \tag{27}$$

$$w^s = \frac{j}{\omega\mu_0}\sum_{n=1}^{\infty}(-j)^n \frac{2n+1}{n(n+1)}\sin\varphi P_n^1(\cos\theta)[j_n(k_h\rho) - b_n h_n^{(2)}(k_h\rho)], \tag{28}$$

$$a_n = \frac{\varepsilon_{r,h} j_n(k_h a) j_n'(k_x a) - \varepsilon_{r,x} j_n(k_x a) j_n'(k_h a)}{\varepsilon_{r,h} h_n^{(2)}(k_h a) j_n'(k_x a) - \varepsilon_{r,x} j_n(k_x a) h_n'^{(2)}(k_h a)}, \tag{29}$$

$$b_n = \frac{j_n(k_x a) j_n'(k_h a) - j_n(k_h a) j_n'(k_x a)}{j_n(k_x a) h_n'^{(2)}(k_h a) - h_n^{(2)}(k_h a) j_n'(k_x a)}, \tag{30}$$

where v^s and w^s are the Debye potentials, a_n and b_n are the scattering coefficients, $P_n^1(x)$ are associated Legendre polynomials, and $j_n(x)$ and $h_n^{(2)}(x)$ are the spherical Bessel functions of the first kind and the spherical Hankel functions of the second kind, of order n, respectively. The scattered field on a circle with radius $b > a$ in the xz-plane is obtained from (26) by putting $\varphi = 0$ and $\rho = b$.

Maxwell–Garnett Formula

The effective permittivity obtained with the full-wave homogenization technique as described in the previous sections can be compared with values predicted by mixing formulas from the classical homogenization approach, which generally are valid for sufficiently low frequencies and volume fractions (Sihvola, 1999). A Maxwell–Garnett formula for randomly oriented PEC spheroids in a dielectric host is given by (Van Damme et al., 2004)

$$\varepsilon_{r,eff} = \varepsilon_{r,h}\left[1 + \frac{f_v}{3(1-f_v)}\left(\frac{1}{N_1} + \frac{1}{N_2} + \frac{1}{N_3}\right)\right]. \tag{31}$$

For a prolate spheroid with semi-axes $a_1 > a_2 = a_3$, the depolarization factors are given by

$$N_1 = \frac{1-e^2}{2e^3}\left(\ln\frac{1+e}{1-e} - 2e\right), \tag{32}$$

$$N_2 = N_3 = \frac{1-N_1}{2}, \tag{33}$$

where $e = \sqrt{1 - 1/A_s^2}$ is the eccentricity and $A_s = a_1/a_2$ is the aspect ratio of the spheroid (Sihvola, 1999; Durand, 1966). In Van Damme et al. (2004), the simple expression (31) is used to invert experimental permittivity data for the fiber content of a few SFRC slabs. This inversion strongly depends on the aspect ratio A_s of the spheroid, which is chosen to model the fiber shape and is actually a cylinder with tiny bends at the ends. In Van Damme et al. (2004) this spheroid is chosen to have the same length and volume as the fiber,

$$a_1 = \frac{l}{2}, \tag{34}$$

$$v_{spheroid} = v_{fiber}, \tag{35}$$

hence the volume fraction f_v is not modified but the aspect ratio of the spheroid $A_s = \sqrt{2/3}l/d$ is smaller than that of the fiber l/d. With the full-wave homogenization technique proposed in this paper, it is possible to examine the validity range of (31) and to further optimize the choice of the spheroid geometry.

Numerical Results

In this section the homogenization approach is tested with numerical examples and the influence of various parameter choices on the fitted effective relative permittivity is illustrated, such as the dimensions of V_{wire}, the illumination frequency, and the radius of the observation circle. Unless specified otherwise, the wires have a length $l = 30$ mm and a diameter $d = 0.55$ mm, hence $l/d = 54.55$ and they are embedded in lossless dry concrete with relative permittivity $\varepsilon_{r,h} = 5.45$. The number of plane waves incident on V_{wire} is $P = 16$ and the number of observation points on the circle is $Q = 16$. For the frequencies that are considered, the wavelength in the host medium λ_h is sufficiently large with respect to l to use only one basis function, $N_b = 1$, in the moment discretization (9). The maximum number of wires is then $N = 5000$ with a Pentium III 1133 MHz, 2 GByte RAM. The approximation (22) for the interaction matrix elements is applied.

Figure 4 shows the influence of the radius of the observation circle on $\varepsilon_{r,eff}$, when V_{wire} is a finite cylinder or a sphere. The frequency is 500 MHz, hence $\lambda_h = 257$ mm. In the lower curves (plain lines) the volume fraction is $f_v = 5.925\ 10^{-4}$ (5 kg/m^3). The crosses there are obtained from a cylinder with radius $a = 87.5$ mm and height $H = 2.5$ m, containing $N = 5000$ wires, and the circles are obtained from a sphere with radius $a = 100$ mm, containing $N = 349$ wires. With the cylinder, a stable value $\varepsilon_{eff} = 6.14$ is obtained when $a < b < 4\lambda_h$; for larger values of b deviations appear, which result from an increasing discrepancy between the fields scattered by the three-dimensional V_{wire} and two-dimensional V_{hom} cylinders. With the sphere the same stable value $\varepsilon_{eff} = 6.14$ is obtained for all values of b. In the higher curves (dashed lines) the volume fraction is doubled, or $f_v = 1.185\ 10^{-3}$ (10 kg/m^3). The crosses there are obtained from a cylinder with the same radius $a = 87.5$ mm but with half the height $H = 1.25$ m as the previous cylinder, containing $N = 5000$ wires, and the circles are obtained from a sphere with radius $a = 100$ mm, containing $N = 698$ wires. It can be seen that with this shorter cylinder, the range of b values that yield a stable value for $\varepsilon_{r,eff}$ is reduced to $a < b < 2\lambda_h$. Results for the sphere are again very stable for all b values. A typical cost function (5) is depicted in Figure 5, which shows a well-pronounced unique minimum.

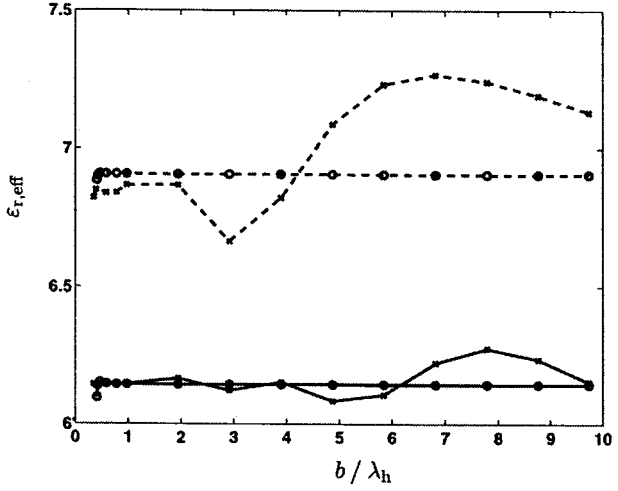

Figure 4. The effective permittivity as a function of the normalized radius of the observation circle for the cylindrical (x) and spherical (○) volumes, and for two volumes fractions, $f_v = 5.925\ 10^{-4}$ (—) and $f_v = 1.185\ 10^{-3}$ (– –).

Figure 6 shows $\varepsilon_{r,eff}$ as a function of the radius of the sphere, for different volume fractions ($f_v = 5.925\ 10^{-4}$, $1.185\ 10^{-3}$, $2.37\ 10^{-3}$, $4.7\ 10^{-3}$) and different frequencies between 100 MHz and 1 GHz. Due to the limitation on the maximum number of wires, the maximum possible radius decreases from 0.24 m to 0.1 m with the increasing volume fractions. For $f_v = 5.925\ 10^{-4}$, a constant relative effective permittivity value is obtained for radii between 0.06 m and 0.24 m (the diameters of the spheres then range from $0.1\lambda_h$ to $1.12\lambda_h$) and for frequencies between 100 MHz and 300 MHz. The mean value and standard deviation over these radii and frequencies are given by $\varepsilon_{r,eff} = 6.12 \pm 0.02$. At 500 MHz and 1 GHz, the values are $\varepsilon_{r,eff} = 6.16 \pm 0.02$ and $\varepsilon_{r,eff} = 6.34 \pm 0.02$, respectively. The result thus deteriorates when the wavelength λ_h is not sufficiently large

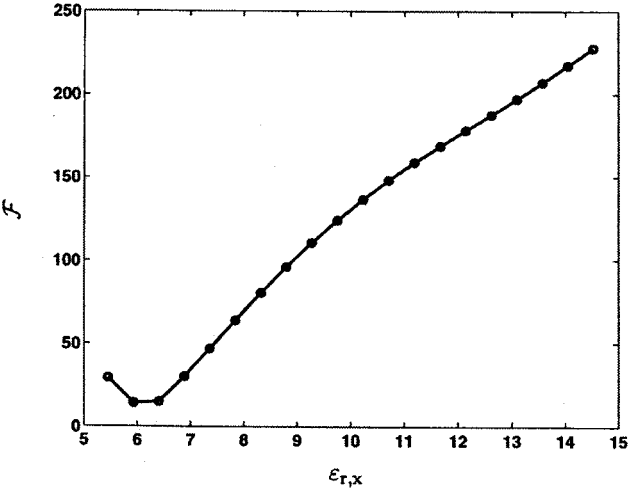

Figure 5. Typical cost function.

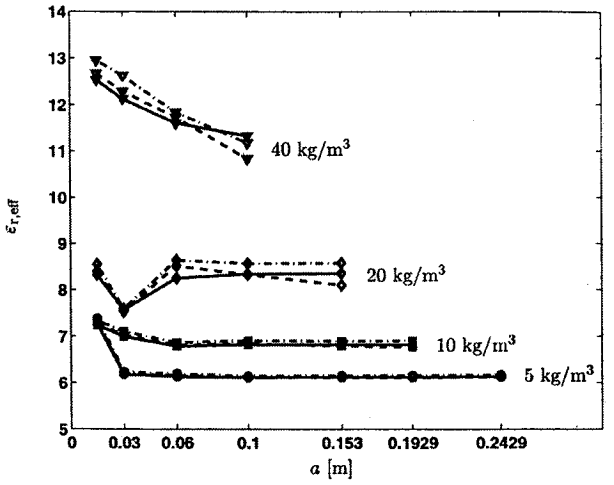

Figure 6. $\varepsilon_{r,eff}$ as a function of the radius of the sphere a for (i) different volume fractions: $f_v = 5.925\ 10^{-4}$ (○), $f_v = 1.185\ 10^{-3}$ (□), $f_v = 2.37\ 10^{-3}$ (◇), $f_v = 4.7\ 10^{-3}$ (▽); and (ii) different frequencies: 100 MHz (—), 300 MHz (– –), 500 MHz (– · –).

with respect to l and when the radius is smaller than 0.06 m. With the volume fractions $f_v = 1.185\ 10^{-3}$ and $f_v = 2.37\ 10^{-3}$ the results are $\varepsilon_{r,eff} = 6.81 \pm 0.03$ and $\varepsilon_{r,eff} = 8.32 \pm 0.17$, respectively. With the higher volume fractions, variations on the permittivity thus become somewhat larger. It can be concluded that spheres need not be large to reach good results. For the highest volume fraction $f_v = 4.7\ 10^{-3}$, the effective permittivity is not constant within the ranges that are considered. This behavior will be studied in future work.

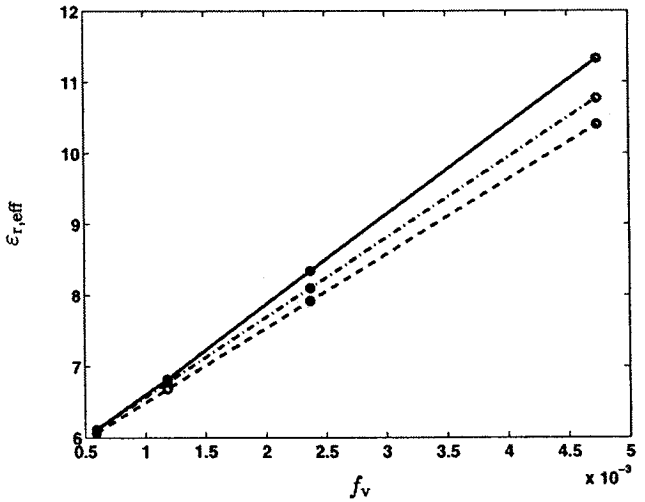

Figure 7. $\varepsilon_{r,eff}$ as a function of the volume fraction: full-wave homogenization (—), Maxwell–Garnett with choice (34), (35) for spheroids (– –), Maxwell-Garnett such that $\varepsilon_{r,eff}$ coincides with the full-wave solution for $f_v = 5.925\ 10^{-4}$ (– · –).

In Figure 7 a comparison between the full-wave homogenization and the Maxwell–Garnett formula (31) is given. The plain line shows $\varepsilon_{r,eff}$ as a function of the volume fraction, obtained with the full-wave homogenization using spheres with radius $a = 0.1$ m at 100 MHz. The dashes show the permittivity obtained with the Maxwell–Garnett formula and with dimensions of the spheroids according to (34)–(35). It can be seen that Maxwell–Garnett yields lower values than the full-wave homogenization. For the volume fraction $f_v = 1.185\ 10^{-3}$, for example, the relative difference is 2%. For the lowest volume fraction $f_v = 5.925\ 10^{-4}$, $\varepsilon_{r,eff} = 6.07$ with Maxwell–Garnett and $\varepsilon_{r,eff} = 6.11$ with the full-wave homogenization. The relative difference here is only 0.7%. A different choice than (34)–(35) for the dimensions of the spheroids is obtained by taking $\sum_{i=1}^{3} 1/N_i = 614.5$ in (31). In this case, $\varepsilon_{r,eff} = 6.11$ also with Maxwell–Garnett, for $f_v = 5.925\ 10^{-4}$, yielding the dash-dot line in Figure 7. The discrepancy between the two effective permittivities has dropped to 0.7% for the volume fraction $f_v = 1.185\ 10^{-3}$.

Finally, some additional verifications are performed for a sphere with $f_v = 2.37\ 10^{-3}$. It follows that $\varepsilon_{r,eff} = 8.2921$ when using the exact expression (17) and $\varepsilon_{r,eff} = 8.2921$ when using the approximation (22), but $\varepsilon_{r,eff} = 8.5805$ when interactions are neglected altogether. It also follows that the results remain stable when repeating the computations for different random realizations, e.g., $\varepsilon_{r,eff} = 8.32 \pm 0.13$ for 10 realizations. When reducing the size of the fibers to $l = 15$ mm, $d = 0.275$ mm, while keeping the aspect ratio A_s and volume fraction f_v unchanged, $\varepsilon_{r,eff} = 8.29$ remains close to a previously obtained result of $\varepsilon_{r,eff} = 8.35$.

Conclusion

A full-wave technique for the homogenization of steel fiber reinforced concrete was presented. The relative permittivity of a homogeneous volume, such as a two-dimensional cylinder or a sphere, was fitted to scattered field data of a wire medium volume, such as a three-dimensional cylinder or a sphere, respectively. With the two-dimensional cylinder the analytical solution is simple, but the dimensions of the finite wire medium cylinder and the locations of the scattered field data need to be chosen with care. Therefore, the sphere is the preferred geometry. For volume fractions corresponding to a fiber density of 20 kg/m^3 or lower, constant values for the effective permittivity are obtained independent of the frequency and of the radius of the sphere, provided that the wavelength is sufficiently large with respect to the length of the fiber and that the radius is at least twice the length of the fiber. It may then be computationally advantageous to select the smallest possible sphere and the lowest frequency. These values also show a satisfactory agreement with a Maxwell–Garnett mixing rule for randomly oriented perfectly conducting prolate spheroids. The proposed method can be used to derive improved mixing rules, e.g., to invert measured effective permittivity data for the fiber content.

References

Burke, G. J., & A. G. Poggio. 1981. *Numerical electromagnetics code (NEC)—Part II: Program description.* Livermore, CA: Lawrence Livermore National Laboratory.

Durand, E. 1966. *Electrostatique—Tome III*, pp. 241–244. Paris: Masson.

Harrington, R. F. 1968. *Field computations by moment methods.* New York, Macmillan.

Harrington, R. F. 2001. *Time-harmonic electromagnetic fields*, 2nd ed. New York: Wiley-IEEE Press.

Milovanovi, G. V., & D. M. Velikovi. 2001. Quadrature processes for several types of quasi-singular integrals appearing in the electromagnetic field problems. In *5th International Conference on Applied Electromagnetics (PES2001)*. Philadelphia: Taylor and Francis.

Nguyen, T. T., & G. Mazé-Merceur. 1998. Microwave characterization of 2-D random materials: Numerical simulations and experiments. *IEEE Trans. Microwave Theory Tech.* 46:1478–1483.

Press, W. H., B. P. Flannery, S. A. Teukolsky, & W. T. Vetterling. 1988. *Numerical recipes: The art of scientific computing*. Cambridge, UK: Cambridge University Press.

Sarabandi, K., & P. R. Siqueira. 1997. Numerical scattering analysis for two-dimensional dense random media: Characterization of effective permittivity. *IEEE Trans. Antennas Propagat.* 45:858–867.

Sihvola, A. 1999. *Electromagnetic mixing formulas and applications*. London: Institute for Electrical Engineering.

Siqueira, P. R., & K. Sarabandi. 2000. T-matrix determination of effective permittivity for 3D dense random media. *IEEE Trans. Antennas Propagat.* 48:317–327.

Taerwe, L., S. Van Damme, & A. Franchois. 1999. Quantification of variations in the steel fibre content of fresh and hardened concrete. In *Proceedings of the Third RILEM Workshop High Performance Fiber Reinforced Cement Composites*, pp. 213–222, Mainz, Germany.

Van Bladel, J. 1985. *Electromagnetic fields*. New York: Hemisphere Publishing Corporation.

Van Damme, S., A. Franchois, D. De Zutter, & L. Taerwe. 2004. Non-destructive determination of the steel fiber content in concrete slabs with an open-ended coaxial probe. *IEEE Trans. Geoscience Remote Sens.* 42:2511–2521.

Weisstein, E. W. 1999. Sphere point picking. From *Mathworld*, A Wolfram Web Resource, http://mathworld.wolfram.com/SpherePointPicking.html.

Volume 26 Numbers 3–4

ISSN: 0272-6343

April–June 2006

ETRMDV 26(3–4) (2006)

electromagnetics

Taylor & Francis
Taylor & Francis Group